

EFFICIENT UNDERGROUND OBJECT DETECTION FOR  
GROUND PENETRATING RADAR SIGNALS

Corresponding Author

İbrahim Meşecan,

imesecan@mevlana.edu.tr

Mevlana University-Konya, Turkey

+355 4 2232 086

Author

İhsan Ömür Bucak,

iobucak@melikshah.edu.tr

Melikşah University-Kayseri, Turkey

+90 352-207 7300

## ABSTRACT

Ground Penetrating Radar (GPR) is one of the common sensor system for underground inspection. GPR emits electromagnetic waves which can pass through objects. According to the properties of the passing medium, these waves are reflected back more or less. The reflecting waves are recorded and digitized, and then, GPR images are formed. According to the properties of the object if it reflects more waves, it creates higher intensity values. Thus, these changes in signal represent the properties of the object being captured. In this paper, the effects of normalization and “3-rows average-subtraction” method have been studied. According to the results, proposed method has increased object detection and true positive object discrimination significantly. For KMeans algorithm, true positive object discrimination has increased from 61% to 81%. And similarly, when K-Nearest Neighbors algorithm is used, true positive object discrimination has increased from 84.4% to 95.7%.

Keywords: GPR, B-scan images, Image processing, Object detection, 3-rows average subtraction.

## INTRODUCTION

First usage of landmines dates back to 13<sup>th</sup> century when Chinese used contact fused land mines to stop Mongols [1]. Land mines are mostly placed between countries in war times. It is reported that more than a hundred million land mines exists in more than 80 countries [2]. And every year, mostly civilians, more people are being killed or injured because of them [3]. After the start of World wars, many countries started using land mines more. And as a result, underground object detection has become more important [1].

The detection of land mines problem is a difficult process due to many factors: large variety of land mine types, different terrain, or weather conditions, and human or natural waste, etc. [4]. Because of the fact that many modern land mines contain little or no metal, traditional field detectors (MD) cannot produce any good results [5]. Some sensors for underground inspection include acoustics and quadruple resonance (QR), ground penetrating radar (GPR), electromagnetic induction sensing (EMI) and neutron backscattering [6]. Recently, Ground penetrating radar (GPR) has become one of the commonly used sensors for many researchers [7] [8] [3].

Mine detection using GPR data and signal processing techniques has a long history [9]. The signals gathered from sensing devices are processed using different signal and image processing techniques. Some are background removal [10], Hidden Markov Models (HMMs) [11] [12], using frequency domain features [3], Fuzzy K-Nearest Neighbors [4], Edge Histogram Descriptors [13], and adaptive approaches for anomaly detection [14], etc.

Due to the real-time requirements many researchers developed two staged algorithms: pre-screening and feature-processing stages. The first phase aims to detect potential interest points quickly and it passes them to a more detailed algorithmic processor. Torrione et al. report that feature-based processor helps to reduce false alarm rate significantly while keeping the probability of detection the same [6].

Gader et al [8] propose feature-based rules, order statistics, and adaptive whitening (FROSAW) and they report that ‘feature based methods outperformed energy detectors’. Frigui et al [13] [3]

proposed to use Edge Histogram Descriptors (EHD). They use a simple edge operator to identify and group edges. They claim that EHD helps to reduce false alarm rate without affecting the detection rate.

## METHODOLOGY

### 1. Dataset used

The dataset has been provided by The Information Technologies Institute of The Scientific and Technological Research Council of Turkey (TUBİTAK) - Gebze, Kocaeli. The data has been collected on two different days:

- using soft soil and 1 GHz GPR signals
- for two types of objects: Metal and Plastic,
  - 10 - 25 cm diameter and 4 cm high metal discs
  - 5 liter standard cylindrical plastic container
- for different object depths: 3, 10, 20, 30 and 40 cm,
- and for different antenna heights: 5, 10, 15 and 20 cm.

There are also some images which have been captured when there is no test object. First A-scan signals are captured [15] [16] (Figure 1).

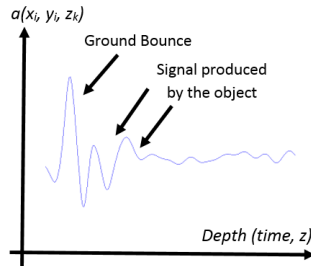


**Figure 1: A-scan signal**

To have better signal to noise ratio (SNR), every point is scanned several times ( $R$  - usually 4 or 8). Then, the signal is digitized and averaged for every point [15]. And thus, the signals have been digitized into 65536 steps (2 bytes intensity resolution).

$$a_A(x, y, z) = \frac{1}{R} \sum_{r=1}^R a(x, y, z) \quad (1)$$

Finally, A-scan signals are combined to form the B-scan images. In Figure 2 below, you can see a sample GPR image that contains a metal object under 3 cm deep.

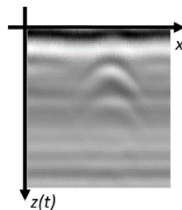


**Figure 2: GPR signal captured for a metal object which is buried under 3 cm.**

Ten GPR images have been collected for every object depth and antenna height. Then, the images have been classified into three categories;

- 1- True positive images: images which contain query object whose type and position are known,
- 2- True negative images: images which do not contain any query object,
- 3- Images which contain a query object but whose position are not recorded.

For exact comparison of the results coming from the proposed algorithm, the images whose object positions are not recorded have not been used in the tests.

The sensing limit of GPR devices change according to the frequency used [17]. In many other researches [11] [18] [7], the objects are buried less than 10 inches deep. But in this research there are some objects which are buried 40 cm deep. When an object goes beyond the sensing limits of GPR sensors, the object cannot be captured in the signal. This can be seen in Figure 3 through the images in which the object depths are 20 - 30 cm and antenna heights are 10, 15 and 20 cm.

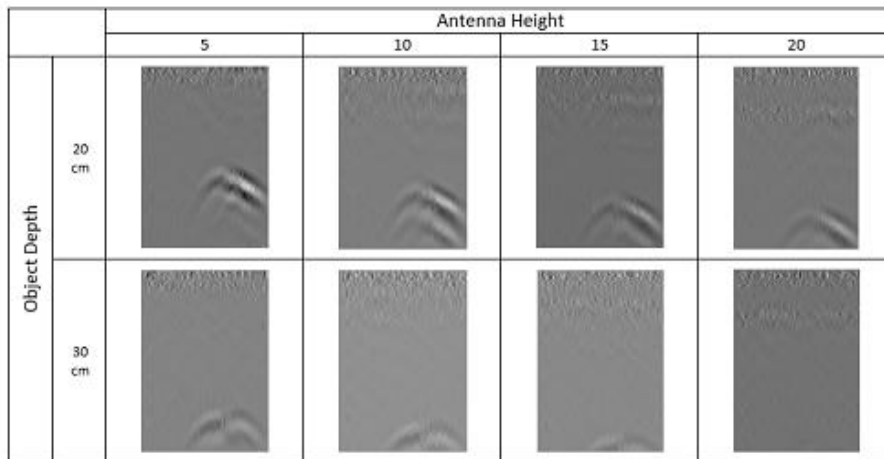


**Figure 3: GPR signals taken from different depths and antenna heights.**

In Figure 3, the object used in all scans is the same object. But because the object depth and antenna height change, the object is captured in deeper positions. And after a point the object disappears from the visible scene. As a result, we have used also these images as True Negatives.

Thus, we have the following number of images in three categories:

1. 310 True Positive (TP) images:
  - a. 250 Metal objects,
  - b. 60 Plastic objects.
2. 180 True Negative (TN) images,
3. 260 True positive images whose positions are not known.

## 2. 3-Rows average subtraction

Sometimes, visualizing images according to their intensity levels can help to see and understand them better. When colored, peaks and holes in the image can be seen better.

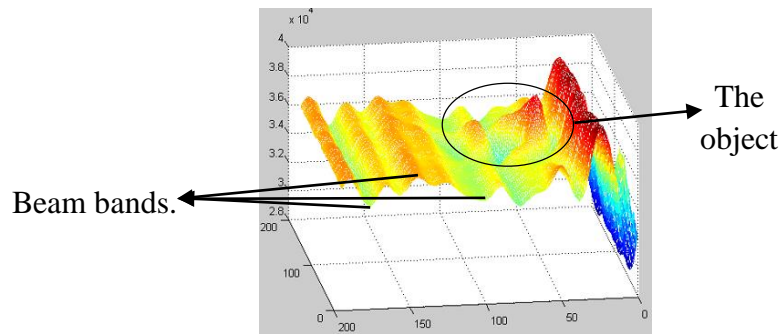


**Figure 4: An example of coloring images according to the intensity levels.**

When GPR signals pass through a medium with the same properties, they are reflected back with the same signal levels. This produces same signal levels like the bands which can be seen in Figure 4. When the beams pass through different medium, they are returned with different peaks (higher intensity levels on a region compared to the pixels around) or holes in the signal. These peaks and holes serve as a signature of the object being captured.

The parallel bands show the extra information that does not contain object specific information. The peaks and holes represent the objects. When the average of the current, preceding and the next rows (3-rows) is subtracted from every pixel intensities of this row, the real object information (peaks and holes) is left and extra information is removed from the signal. One can think that the average of current row should produce better results. However, the average of current row is too much affected from the holes or peaks in that row.

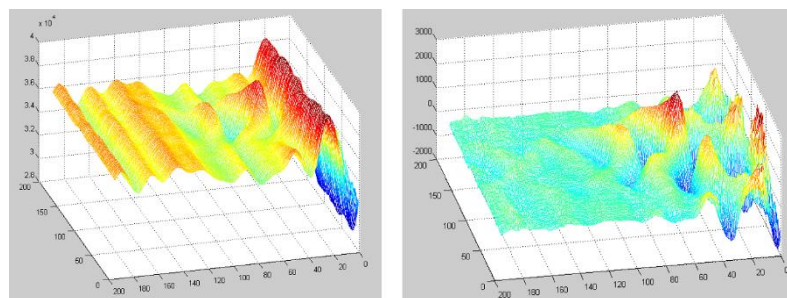


**Figure 5: a) A plastic object buried under 10 cm deep  
b) After subtracting the average of 3-rows.**

Figure 5 above shows the images before and after 3-rows average subtraction. The intensity range before 3-rows average subtraction is between 27000 and 42000. And, it changes from -2000 to 2500 after 3-rows average subtraction. This is important because a peak of 2000 out of 5000 will have more meaning than a peak of 7000 out of 42000 (higher SNR). Moreover, 3-row average subtraction method preserves most of signal properties while removing extra information.

These signatures are preserved even after significant image scaling [19]. The image below in Figure 6 contains processed image from Figure 4. The image has been normalized using 3-rows average subtraction (the left image). Thereafter, it has been scaled to 25% and Min-Max normalized (the right image).

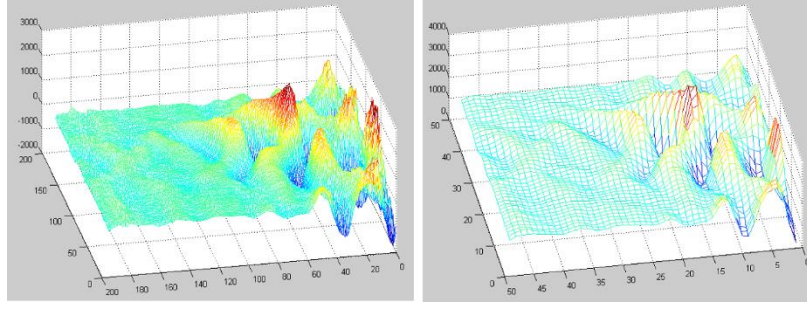


**Figure 6: a) the image after 3-rows average subtraction  
b) the image scaled to 25% and normalized between 0 and 4000.**

## IMPLEMENTATION AND RESULTS

We have analyzed the effects of 3-rows average subtraction using two common algorithms: KNN and KMeans which are in top ten algorithms in Data mining for many researchers [20].

### 1. Implementation using KMeans

In our tests, GPR images contain 256-by-180 (height-by-width) pixels where the height represent the depth of the captured signal. Objects usually create a 60-by-90 (height-by-width) signature in the image. Because we have a small dataset, to populate it, we have cropped 60-by-90 images from the existing negative images. Hence entire image is negative (no query object in it), any part of the image can be cropped as a new negative image. And thus, we have cropped 12 (60-by-90) images from random coordinates of every True Negative (TN) image and produced a set of 2160 TN (180x12) images.

However, True positive images cannot be reproduced with the way we have populated negative images. To produce more sets, we run the program 20 times. And, in every run, the order of images have been shuffled randomly to construct different test and data sets: as a total of 49400 test images (20 x (2160 + 310) ).

Finally, we have repeated the same process for different scale sizes: 50%, 33%, 25%, etc. [19]. Table 1 below has been produced with the conditions described below

- KMeans with k=3; three classes: Metal objects, Plastic objects and none exists
- for 2160 TN and 310 TP (250 Metal and 60 Plastic objects),
- 60-by-90 image crops have been scaled to 25% (to 15-by-22 after scaling),
- program run 20 times producing 20 different test sets,
- Intensity level of every image has been Min-Max normalized between 0 and 4000.
- Without 3-row average subtraction

**Table 1: Confusion matrix, Object discrimination for KMeans.**

		Object found		
		Metal	Plastic	Nothing
Object is	Metal	3439	793	768
	Plastic	181	281	738
	Nothing	2361	11973	28866

KMeans has identified 3439 metal objects correctly as metal objects; 793 metal objects have been misclassified as Plastic and 768 metal objects have been misclassified as nothing. Thus, (3439 + 281 + 28866) 32586 images out of 49400 ((2160 + 310) x 20) have been identified correctly. That is 66% of all objects have been classified correctly. For True Positive object discrimination (TPOD), (3439+281) 3720 of the positive images have been classified correctly out of (20x310) 6200 samples. This gives 60% True positive object discrimination accuracy where

$$TPOD = \frac{Nr\ of\ positive\ images\ identified\ correctly}{Nr\ of\ all\ positive\ images} \quad (2)$$

Figure 7 below has been produced with the same conditions given above for Table 1, for below mentioned scaling and normalization.

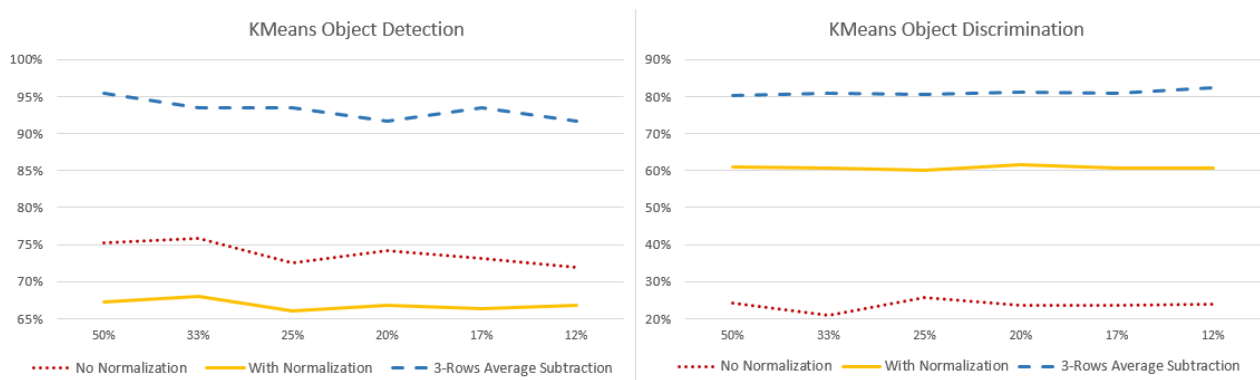


**Figure 7: KMeans object detection (left) and TPOD (right).**

From the figure above, it is seen that scaling does not affect the detection process much [19]. And it gives nearly the same results for all scalings when normalized or processed with 3-rows average subtraction.

In the left image, though, min-max normalization seems to have a bad effect on object detection, and thus, the average object detection (for all scalings) has dropped from 73.8% to 66.9%. However, it has increased true positive object detection from 23.6% to 60.7%.

It is also seen that 3-rows average subtraction has great positive influence on object detection: the average object detection for all scales has increased from 66.9% to 93.2% (left image). Similarly, TPOD after 3-rows average subtraction has increased from 60.7%, to 81%. This shows that 3-rows average subtraction has a clear positive effect on both: object detection and discrimination processes.

## 2. K-Nearest Neighbors (KNN)

We have repeated the tests using K-Nearest Neighbors. Hence KNN is a supervised learning algorithm, we have divided the dataset into 70% training and 30% test sets. Because we have a small set (only 310 true positive images), to produce more test elements, we have run the program many times while shuffling the training and test set elements randomly. Table 2 below has been produced with the following conditions:

- KNN with k=8; class of testing object is decided according to 8 nearest neighbors
- for 2160-TN and 310-TP,

- 60-by-90 image crops have been scaled to 25% (to 15-by-22 after scaling),
- program run 14 times producing 14 different test and data sets,
- each run has randomly separated the data into 70% dataset 30% test set,
- Intensity level of every image has been Min-Max normalized between 0 and 4000.

**Table 2: Confusion matrix, Object discrimination for KNN.**

		Object found		
		Metal	Plastic	Nothing
Object is	Metal	996	54	0
	Plastic	0	134	118
	Nothing	41	0	9031

KNN has identified 996 metal objects correctly as metal objects; 54 metal objects have been misclassified as Plastic. Thus, from 10374 (741 test images and 14 runs) test images (996 + 134 + 9031) 10161 images have been identified correctly, and (54 + 118 + 41) 213 of them have been misclassified. That is, 97.9% objects have been detected correctly. For TPOD, (996+134) 1130 out of 1302 of TP images have been classified correctly which gives 86.8% True positive object discrimination accuracy.

Figure 8 below has been produced with the same conditions given above for Table 2, for the below mentioned scaling and normalization.

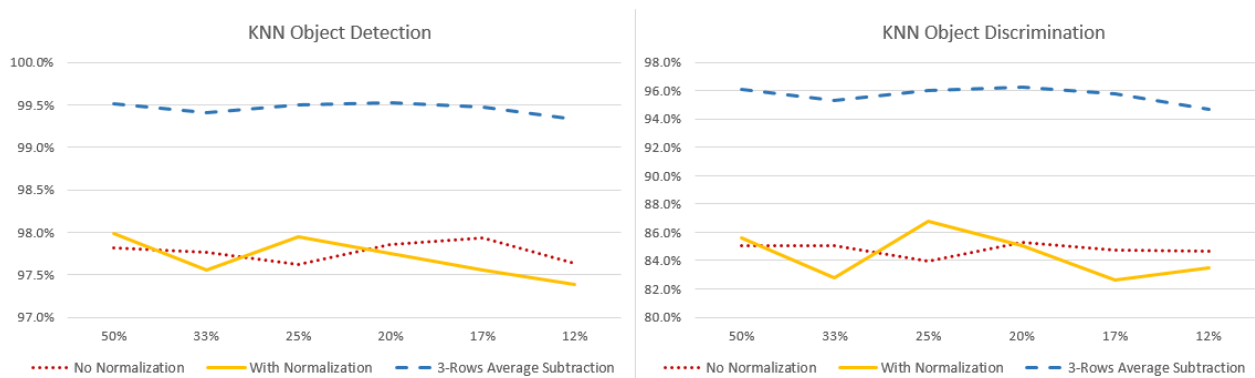


**Figure 8: KNN object detection and discrimination.**

Min-max normalization alone has nearly no effect on object detection and discrimination. The average object detection percentage for all scaling sizes without normalization is 97.8% and with normalization is 97.7%. On the other hand, after 3-rows average subtraction, it reaches to 99.5%. The effect of 3-rows average subtraction can also be seen from the TPOD ratios:

- TPOD is 84.8% when there is no normalization.
- With min-max normalization, it goes down to 84.4%.
- And after 3-rows average subtraction TPOD increases to 95.7%.

## CONCLUSION

Landmine detection is still very important for many countries in the world. It requires fast and accurate detection performance. Usually, being fast and accurate contradicts with each other. This paper targets fast and accurate processing. 3-rows average subtraction has increased both object detection and True positive object discrimination percentages significantly. The positive effects of 3-rows average subtraction is clearly seen for both algorithms. For KNN, TPOD has increased from 84.8% to 95.7%. When KMeans algorithms is applied, although, simple min-max normalization increases TPOD, but the object detection decreases to 66.9%. However, when 3-rows average subtraction is applied, both object detection and object discrimination increases significantly.

The images which are min max normalized have produced, on the average for all scale sizes, 84.4% accuracy with a standard deviation of 1.53 on different object scalings for True positive object discrimination; while 3-rows average subtraction, images have produced 95.7% accuracy with a smaller standard deviation of 0.53. According to our observations, the variations in the results can be due to 1) small data set used and 2) random test cases used. The experiment can give better opinion with three dimensional data and large number of true-positive datasets.

## References

- [1] R. Siegel, "Land Mine Detection," *IEEE Instrumentation & Measurement Magazine*, pp. 22-28, December 2002.
- [2] U. Nations, "Landmines, mine action news from the united nations," United Nations, New York, 1998.
- [3] H. Frigui and P. Gader, "Detection and discrimination of land mines in ground-penetrating radar based on edge histogram descriptors and a possibilistic k-nearest neighbor classifier," *IEEE Transactions on Fuzzy Systems*, vol. 17, no. 1, pp. 185-199, 2009.
- [4] H. Frigui, P. Gader and K. Satyanarayana, "Landmine Detection with Ground Penetrating Radar using Fuzzy K-Nearest Neighbors," in *IEEE International Conference on Fuzzy Systems*, Budapest, 2004.
- [5] K. C. Ho, P. D. Gader and J. N. Wilson, "Improving landmine detection using frequency domain features from ground penetrating radar," in *Geoscience and Remote Sensing Symposium, IEEE International*, Anchorage, AK, 2004.
- [6] P. A. Torrione, C. S. Throckmorton and L. M. Collins, "Performance of an Adaptive Feature-Based Processor for a Wideband Ground Penetrating Radar System," *IEEE Transactions on Aerospace and Electronic Systems*, vol. 42, no. 2, pp. 644-658, 2006.
- [7] H. Frigui, L. Zhang, P. Gader and D. Ho, "Context-dependent fusion for landmine detection with ground-penetrating radar," in *Defense and Security Symposium*, Orlando, FL, 2007.
- [8] P. Gader, W. H. Lee and J. N. Wilson, "Detecting Landmines With Ground-Penetrating Radar Using Feature-Based Rules, Order Statistics, and Adaptive Whitening," *IEEE Transactions on Geoscience and Remote Sensing*, vol. 42, no. 11, pp. 2522-2534, 2004.

- [9] D. J. Daniels, "Surface-penetrating radar," *Electronics & Communication Engineering Journal*, vol. 8, no. 4, pp. 165-182, 1996.
- [10] M. Sezgin, F. Kurugollu, I. Tasdelen and S. Ozturk, "Real-time detection of buried objects by using GPR," in *Detection and Remediation Technologies for Mines and Minelike Targets IX*, Orlando FL, 2004.
- [11] J. N. Wilson, P. Gader, W. H. Lee, H. Frigui and K. C. Ho, "A large-scale systematic evaluation of algorithms using ground-penetrating radar for landmine detection and discrimination," *IEEE Transactions on Geoscience and Remote Sensing*, vol. 45, no. 8, pp. 2560-2572, 2007.
- [12] P. D. Gader, M. Mystkowski and Y. Zhao, "Landmine detection with ground penetrating radar using hidden Markov models," *IEEE Transactions on Geoscience and Remote Sensing*, vol. 39, no. 6, p. 1231—1244, 2001.
- [13] H. Frigui and P. Gader, "Detection and discrimination of land mines based on edge histogram descriptors and fuzzy k-nearest neighbors," in *IEEE International Conference in Fuzzy Systems*, Vancouver, BC, 2006.
- [14] P. A. Torrione, L. M. Collins, F. Clodfelter, F. Frasier and I. Starnes, "Application of the LMC algorithm to anomaly detection using the Wichmann/NIITEK ground-penetrating radar," in *AeroSense*, Orlando, FL, 2003.
- [15] M. Sezgin, Y. Bahadirlar and I. Tasdelen, "Signal processing techniques to improve GPR detection performance," in *Detection and Remediation Technologies for Mines and Minelike Targets X*, Orlando, Florida, 2005.
- [16] V. Munshi and L. M. Collins, "Physics model-based signal processing of gpr for subsurface object detection and discrimination," Department of electrical and computer engineering, Duke University, Durham, NC, 2003.
- [17] A. S. Turk, "Ultra- wideband Vivaldi antenna design for multisensor adaptive ground-penetrating impulse radar," *Microwave and optical technology letters*, vol. 48, no. 5, pp. 834-839, 2006.
- [18] C. R. Ratto, K. D. Morton, I. T. McMichael, B. P. Burns, W. W. Clark, L. M. Collins and P. A. Torrione, "Integration of lidar with the NIITEK GPR for improved performance on rough terrain," *SPIE Defense, Security, and Sensing*, vol. 5089, pp. 1375-1382, 2012.
- [19] I. Mesecan and I. O. Bucak, "Searching The Effects of Image Scaling For Underground Object Detection Using KMeans And KNN," in *UKSim-AMSS 8th European Modelling Symposium*, Pisa, 2014.
- [20] X. Wu and V. Kumar, *The top ten algorithms in Data Mining*, Boca Raton, London, New York: Chapman & Hall/CRC Taylor & Francis Group, 2009.

## Competing Interests

“We have read and understood policy on declaration of interests and declare that we have no competing interests.”

## List of abbreviations

EHD Edge Histogram Descriptors

EMI Electromagnetic Induction

FROSAW Feature-based rules, order statistics, and adaptive whitening

GPR Ground Penetrating Radar

HMM Hidden Markov Models

KNN K-Nearest Neighbors

MD Metal Detectors

QR Quadruple resonance

SNR Signal to noise ratio

TN True Negative images

TP True Positive images

TPOD True positive object discrimination

TUBITAK The Information Technologies Institute of The Scientific and Technological Research Council of Turkey